Hindawi
Advances in Civil Engineering
Volume 2019, Article ID 9317910, 9 pages
https://doi.org/10.1155/2019/9317910

Research Article

Spring Deformation Gauge for Measuring Local Deformations in Triaxial Apparatus

Mostafa A. Ismail[1] and Yasser E. Ibrahim[2,3]

[1]*Principal Geotechnical Engineer, CMW Geosciences, Perth, WA, Australia*
[2]*Engineering Management Department, Prince Sultan University, Riyadh, Saudi Arabia*
[3]*Structural Engineering Department, Zagazig University, Zagazig, Egypt*

Correspondence should be addressed to Yasser E. Ibrahim; yibrahim@vt.edu

Received 31 January 2019; Accepted 12 March 2019; Published 1 April 2019

Academic Editor: Salvatore Grasso

Local measurement of deformations of a soil specimen has become inevitable for accurate determination of soil stiffness in triaxial tests. Although there are now many devices that can be used to perform this task, each has its own advantages and limitations that render development of new devices with better desirable features. This paper presents an innovative device called spring deformation gauge (SDG) that has many advantages over many of the existing devices and can be readily manufactured in both research and commercial laboratories. The device is based on using a highly flexible, yet very strong metal strip of spring steel secured between two stiff, stainless steel L-shaped legs; the spring strip is provided with four strain gauges. With this arrangement, local deformation of a specimen is transferred into significant bending in the metal strip and elongation or shortening of the strain gauges. In addition to being very cost effective, the SDG is characterized by the ability to control both range and resolution of measured deformation, its linear output, and a clever pinning mechanism that protects it from being damaged when it goes out of range. Success of the SDG was demonstrated in a true K_0 test on carbonate sand.

1. Introduction

It is well established now that accurate determination of soil deformation parameters such as stiffness and Poisson's ratio nictitates locally measuring the actual deformation of a certain gauge length of a triaxial specimen; the premise of this approach is to avoid errors associated with machine compliance, bedding, and seating errors, which inevitably lead to gross underestimation of soil stiffness (e.g., [1, 2]). The effect of strain rate on the soil stiffness is negligible at small strains, while it has a considerable effect at higher strains [3, 4]. Accordingly, using local measurement of axial deformation of triaxial specimens has almost become routine in majority of research laboratories concerning stiffness.

Two main types of devices are normally used to measure local deformations of a triaxial specimen, namely, contact and noncontact [5]. Examples of the contact type include electro-level gauge [2], linear variable displacement transformers (LVDT) [6], Hall-effect gauges [7], and local deformation transducers (LDT) [8, 9]; examples of the noncontact type include proximity transducers [10] and cylindrical capacitance devices [11]. Similar to submersible mini LVDTs, proximity transducers have a linear range and can achieve good resolution with 12 or 16 bit data acquisition systems. However, compared with the SDT system described here, they are very expensive and cannot be used in water. They are also susceptible to pressure change and exhibit difficulty during setup [12].

Surveying the literature has shown that there is no consensus as to a particularly preferred transducer, since each of the existing ones has its advantages, disadvantages, and limitations [5]. Perhaps, the two most appealing devices nowadays in this category are submersible LVDTs and LDTs; however, these transducers suffer from several limitations as summarised in Table 1.

Table 1: Issues associated with LVDTs and LDTs.

Device	Critical issues (disadvantages/limitations)
Linear variable displacement transformers (LVDT)	(i) Alignment of the transducer inevitably leads to stiff connections that may affect sample behaviour. (ii) Bulky (iii) Potential friction between the moveable iron core (armature) and the internal cage housing the electromagnetic coils, either by misalignment or due to specimen barrelling. (iv) Special arrangements are required to measure radial strain (v) Unless it is of the unguided type, damage may occur if the LVDT goes out of range. (vi) Relatively expensive
Local deformation transducers (LDT)	(i) Nonlinear output (ii) Friction between the gauge strip and the pin connection unto the specimen can change the boundary conditions normally assumed during calibration (iii) Nondurable (iv) Can get damaged during a test when it goes out of range unless a complex mechanism is used to undo it

It follows from the discussion above that despite the success of the various existing devices and the breakthrough they made in understanding the behaviour of geomaterials at small strains, there is a room for innovation in this area.

This paper presents an innovative spring deformation gauge that can be readily used to measure both axial and radial deformations of triaxial specimens. The gauge possesses flexibility that can enable the designer to achieve favourable features by controlling certain parameters. Capabilities of the gauge are demonstrated by presenting results from a true K_0 test performed on uncemented carbonate sand.

2. Description of the Spring Deformation Gauge (SDG)

The spring deformation gauge (SDG) presented in this paper consists of a two L-shaped stainless steel segments (legs) that are connected via a very thin metal strip (Figures 1 and 2). The metal strip is firmly secured via very small screws between the two legs, such that the in-plane (i.e., dotted rectangle in Figure 1) bending stiffness of the strip is much less than that of each of the two legs (Figure 2). This is achieved by ensuring that the thickness of the strip and that of each of the two legs are orthogonal such that the thickness of the leg (normal to the dotted rectangle in Figure 1) is greater than that of the strip, leading to a much higher in-plane inertia for the leg than the for the strip for the same cross sectional area. Therefore, the deformation of these legs due to the specimen's axial or radial shortening or elongation is negligible, and the only deforming element in the SDG is the metal spring in between. Typical axial and radial SDGs used in this study are presented in Figure 3).

Measurement of the spring deformation (and hence that of the specimen) is actually made via an electric circuit of four strain gauges that are glued to both sides of the spring strip to form a full Wheatstone bridge to compensate for possible temperature variation in the testing environment. Another intrinsic advantage of the full bridge is the negligible interference effect within its connections. Locations of the four strain gauges on the proposed SDG strip can be seen in Figure 1.

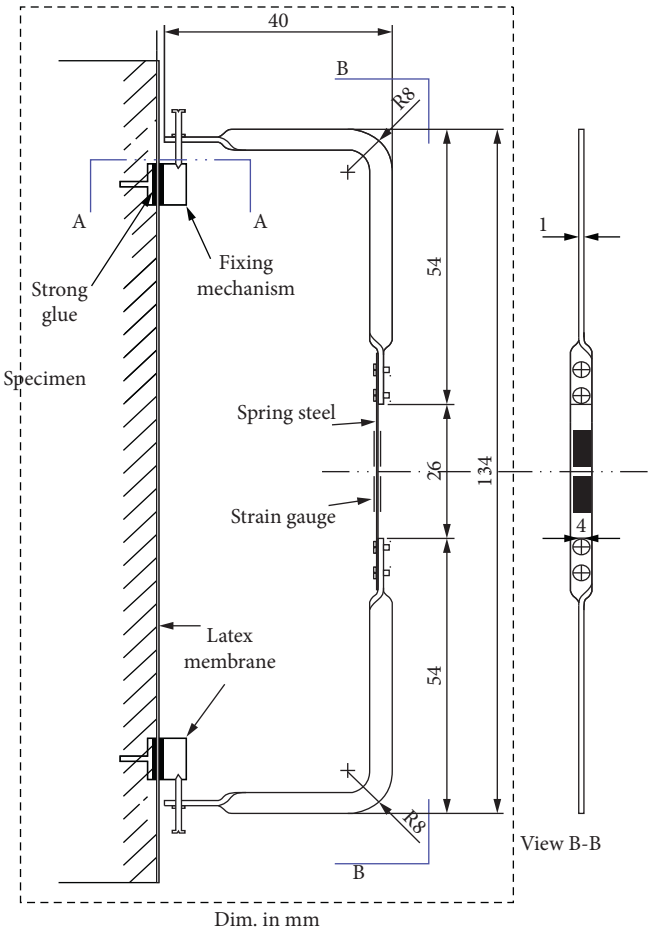

Figure 1: Axial spring deformation gauge used in this study.

3. Parameters Affecting the Spring Deformation Gauge

The following formula determines the relationship between change in length of the gauge strip and the corresponding change in a triaxial specimen (refer to the derivation presented in Appendix and associated notations):

$$\Delta L_{\text{spring}} = \frac{3(EI)_l t_s}{6(EI)_l L_2 + 2(EI)_s (L_2/L_s) L_2} \Delta L_{\text{specimen}}. \quad (1)$$

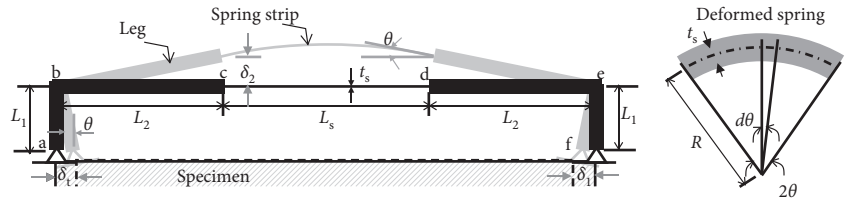

(a) (b)

Figure 2: (a) Schematic showing various components of the axial spring deformation gauge. (b) Curvature of the spring for elongation calculation.

(a) (b)

Figure 3: (a) Typical axial SDG and (b) typical radial SDG used in this study.

Equation (1) can be rewritten as

$$\Delta L_{\text{spring}} = A\Delta L_{\text{specimen}}, \quad (2)$$

where $(EI)_l$ is the product of Young's modulus and section inertia of the gauge leg, $(EI)_s$ is the product of Young's modulus and section inertia of the gauge spring, and A is a gauge multiplier factor, constant for each SDG, reflecting the linearity of the gauge (refer to Figure 4 for the calibration curve of the specific SDG used in this paper). The multiplier A depends on the geometric configuration of the gauge plus the materials of the leg and spring components. The influences of the various parameters affecting A are discussed next.

3.1. Effect of Gauge Geometry. Inspection of equations (1) and (2) reveals that the geometrical parameters that affect the output of the SDG (hence its resolution and maximum range) are the leg length (L_1), spring thickness (t_s), and the leg/spring length ratio (L_2/L_s). Influence of each of these three parameters on the gauge multiplier A is presented in Figure 5, where each of the parameters was varied while maintaining the other two constants. The default values used to produce the results in Figure 4 are listed in Table 2.

Examination of the results presented in Figure 5 shows clearly that the leg length L_1 and the spring thickness t_s can have significant effect on the response of a SDG. This response is inversely proportion to the leg length L_1. On the other hand, the response of the gauge to change in t_s is more complex, since a change in t_s also changes the bending stiffness of the strip. The net result shown from Figure 5 is that the gauge

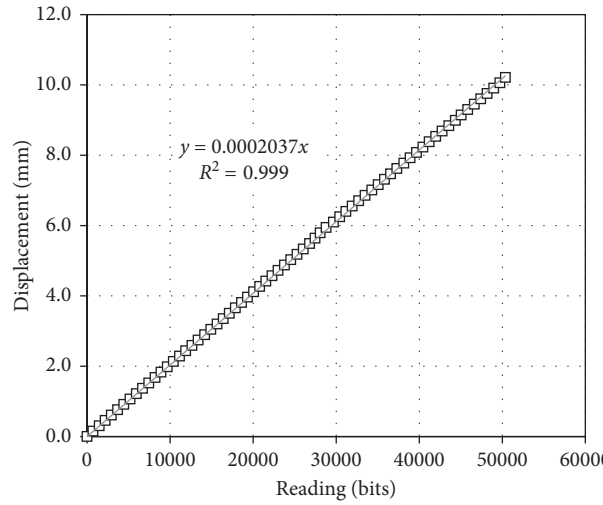

Figure 4: Calibration curve of radial SDG.

multiplier increases with increasing t_s until an optimum value, beyond which the multiplier starts to decrease.

Finally, the result in Figure 5 suggests that the ratio L_2/L_s has practically no effect on the response of the SDG, compared with L_1 or t_s.

3.2. Effect of Gauge Materials. To ensure durability of the SDG and lasting resistance to corrosion, it is inevitable to use stainless steel for the two L-shaped legs. This choice is also

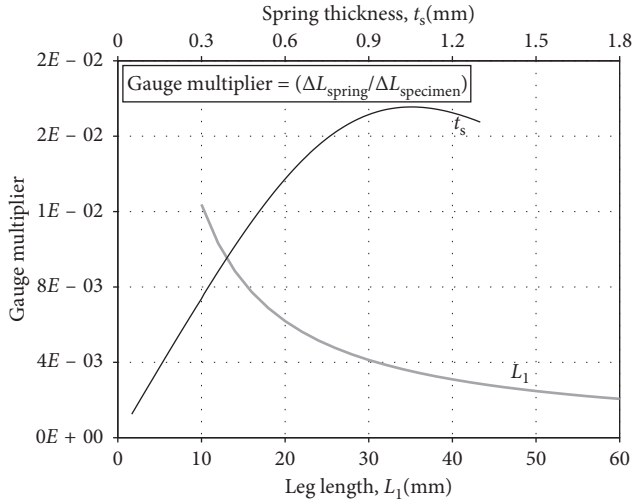

Figure 5: Influence of SDG geometry on its resolution.

beneficial to create very stiff legs relative to the spring, since steel has a high elastic modulus ($E = 210$ GPa), compared with other common metals such as copper or metals (which possess much less resistance to corrosion and hence less longevity).

Since the overall relative stiffness between the middle spring strip and the gauge legs is pivotal for the function of the SDG, it is important to investigate the effect of the material of the spring. To this end, Figure 5 presents the relationship between the gauge amplifier factor (A) and the elastic modulus of the spring material (default values of other parameters are listed in Table 2). The scale of the vertical axis in Figure 6 is deliberately kept consistent with that in Figure 5 to facilitate the comparison. Practically, variation of the values of the deformation modulus between 25% and 200% of that of the gauge leg has negligible effect on the gauge performance (note the relative stiffness stems from the much lower inertia of the metal strip compared with the leg, as indicated earlier).

In fact, the two main factors that characterise performance of the SDG (and other transducers) are the maximum range of deformation that it can cover and the smallest value it can resolve. The latter is normally expressed in terms of strain values. There is agreement with the results found in the literature (e.g., [5]) that local deformation devices should be able to resolve the strain down to 0.001%. The smallest resolution of a transducer is inversely proportional to its maximum range through the following relationship:

$$\text{resolution} = \frac{\text{maximum measurable range}}{\text{number of bits of the measuring system}}. \tag{3}$$

Equation (3), along with the argument above, suggests that an efficient design of SDG should seek optimum outcomes as to both the smallest strain that can be resolved and the maximum range that can be captured by the transducer.

Manipulation of equations (1) and (2) leads to the following expression for the maximum deformation that can be measured by SDG:

$$\text{Max } \Delta L_{\text{specimen}} = \frac{\sigma_y}{E_s} L_s \left(\frac{1}{A}\right), \tag{4}$$

where σ_y is the yield strength (elastic limit) of the spring material.

As was shown above in Figure 6, E_s has negligible effect on the gauge multiplier A. Accordingly, the notion from equation (4) is that the maximum range of deformation that can be resolved by an SDG is directly proportional to the spring length (L_s) and the ratio σ_y/E_s. Table 3 shows the ratio of σ_y/E_s for various metals, with the highest values being in the order of titanium ($\sigma_y/E_s = 0.91$), aluminium ($\sigma_y/E_s = 0.71$), and spring steel ($\sigma_y/E_s = 0.57$). Since titanium is expensive and aluminium has low corrosion resistance, spring steel appears to be ideal for the SDG described here, especially that a very high range possibly associated with a titanium or aluminium gauge can reduce the gauge resolution according to equation (3). In fact, spring steel is typically recommended in similar applications because of its high yield strength, resistance to deformation, and its ability to return to its original shape. The spring steel used in this paper is of type 67SiCr5 [13].

4. Installation Method

In order to connect the SDG to a specimen, each of its two ends is provided with a screw (Figure 7), the tip of which is machined to provide a smooth, conical configuration. The SDG is then carried unto the specimen by housing each of the conical tips into an inverted conical cavity carved into the outer side of a metal (aluminium) bracket glued to the latex membrane enclosing the specimen. Gluing the bracket directly unto the membrane will not produce a robust connection. The setup allows the bracket to be connected to a small insert buried into the sample with the membrane glued to both. This way, the connection of the SDG to the sample will not be affected by any accidental deformation of the membrane. The SDG should be mounted in position while the user applying initial bending moment to the spring in a direction opposite to that anticipated by the specimen deformation during testing; in a triaxial compression test, the SDG should be initially bent so that axial shortening of the specimen will reduce the bending; the opposite should be followed for triaxial extension test. The main advantage of this arrangement is that once the SDG reaches its limiting range, it will experience no bending and will simply fall off the supporting bracket unto the triaxial base. This point is illustrated figuratively in Figure 8 for an axial SDG with a specimen under compression. A radial SDG would be installed and commissioned in the same manner.

5. Application of the New SDG in a K_0 Triaxial Test

5.1. Specimen Preparation and Installation of SDGs. A K_0 triaxial test requires applying a consolidation regime

Table 2: Default values used to produce the relationships in Figure 4.

L_1 (mm)	L_2 (mm)	L_s (mm)	E_l (GPa)	Leg width (mm)	Leg thickness (mm)	E_s (GPa)	Spring width (mm)	Spring thickness (mm)
20	30	30	210	4	1	200	4	0.25

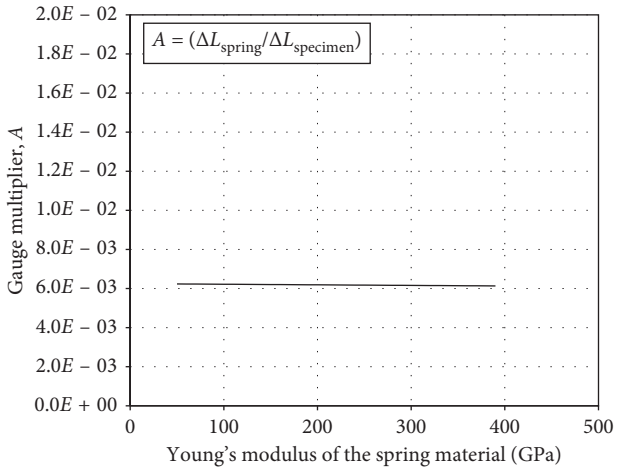

Figure 6: Influence of elastic modulus of the spring material.

Table 3: Ratio of yield strength/Young's modulus for various metals [14].

Metal	σ_y/E_s
Aluminium	0.714
Beryllium	0.147
Brass	0.058
Copper	0.378
Lead	0.206
Nickel	0.500
Stainless steel	0.114
Titanium	0.910
Spring steel	0.571

where both effective vertical and effective radial stresses are continuously adjusted such that the radial strain ε_r is virtually zero. In a test where radial strain measurement is available, feedback from the measuring transducer is used to control both the loading ram and cell pressure to limit the radial strain to an infinitesimally small error (±) that would be maintained during the consolidation phase [15]. In the absence of a local radial strain, the lateral strain is calculated indirectly from measurement of both axial (ε_a) and volumetric strains (ε_v) using the relationship ($\varepsilon_r = (\varepsilon_v - \varepsilon_a)/2$) for triaxial test conditions.

To investigate the two techniques described above for the determination of K_0, a test was performed on carbonate sand from Rottnest Island offshore the coastline of Perth in Western Australia. Details of this soil can be found in [16]. A summary of the physical properties of this soil is presented in Table 4.

The K_0 test was performed on a triaxial specimen of 71.5 mm diameter and 177.5 mm height, prepared to a dry density of 1.32 g/cm^3 by dry pluviation into a membrane stretched inside a split mould. After being assembled unto the pedestal of the triaxial apparatus and subjected

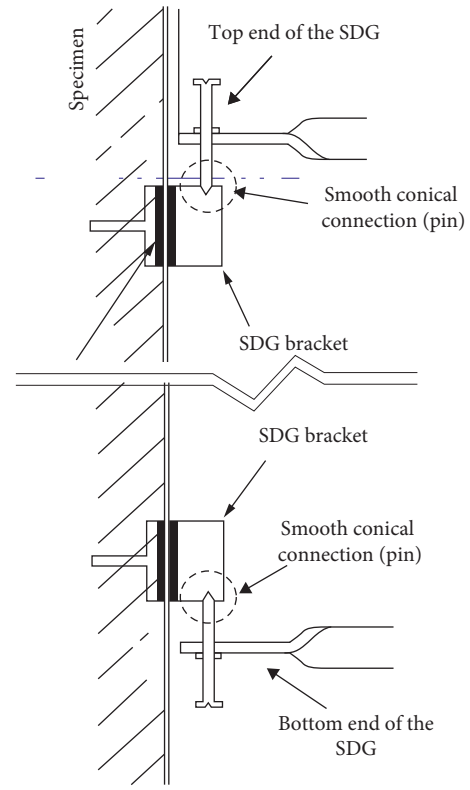

Figure 7: Details showing connection of SDG to specimen.

to small effective stress by vacuum, the specimen was instrumented with one pair of axial SDG and one pair of radial SDG to measure the axial and radial deformations, respectively. The initial bending of each gauge was adjusted by changing the length of the screw pinned to the recess of the mounting bracket glued to the membrane (refer to the photograph in Figure 9). To control the resolution of each of the 4 SDGs, the corresponding gain factor of the data acquisition system was adjusted to produce the values listed in Table 5. In this test, the radial strain that was used to control both cell pressure and axial ram force was determined using the relationship ($\varepsilon_r = (\varepsilon_v - \varepsilon_a)/2$), where ε_a represents the axial strain that was measured by the external LVDT and ε_v represents the volume of water flowing out of the specimen and measured by a commercial pressure volume control unit [17]. In applying these procedures, the permissible radial strain was selected to be 2×10^{-5}, which is approximately the order that can be resolved for the quantity $(\varepsilon_v - \varepsilon_{a\,external})/2$ using the resolution values listed in Table 5.

5.2. Test Results and Discussion. Figure 10 shows response of the various transducers during the K_0 consolidation phase

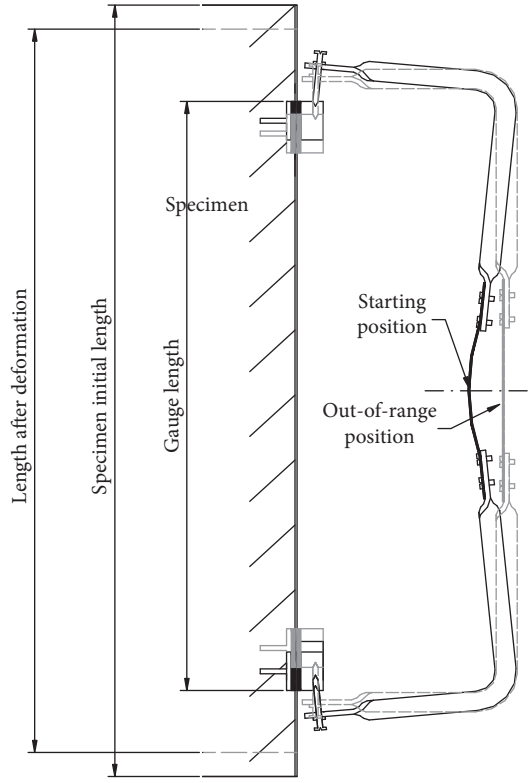

Figure 8: Initial and final positions of the SDG during a compression test.

Table 4: Physical properties of Rottnest sand.

Soil	G_s	D_{10} (mm)	D_{50} (mm)	% fines	e_{max}	e_{min}	$CaCO_3$ (%)
RT	2.70	0.17	0.30	0.8	1.231	0.824	90

(during which the excess pore pressure was monitored to ensure the loading rate was not associated with any buildup of pressure). It is clear that, as expected, the externally measured axial strain ($\varepsilon_{a\,external}$) is virtually equal to the volumetric strain measured by the commercial unit. Interestingly, the maximum radial strain registered by the local SDG gauge ($\approx 3 \times 10^{-5}$) is almost within the error assumed during shearing. Although this value is almost 3 times the resolution of the internal radial SDG listed in Table 5 (which could also even improve further), the overall stress path and resulting K_0 (Figure 11) are satisfactory (i.e., even when the axial strain used to deduce the radial strain was measured externally).

The stress path presented in Figure 11 represents two phases in the triaxial test: (1) K_0 consolidation to cell pressure of 200 kPa, followed by (2) undrained shearing to 20% axial strain. The stress path in Figure 11 plots the deviator stress ($q = \sigma_1 - \sigma_3$) versus the mean effective stress ($p' = (\sigma_1^A + 2\sigma_3^A)/3$). A constant gradient of the K_0-line phase yields $K_{0(NC)} = 0.42$ (note the normally consolidated state of the sand tested here), whereas the ultimate (approximately the critical state) gradient of the undrained shearing phase (Figure 11) yields $\phi_{cv} \approx 37^\circ$. These results are

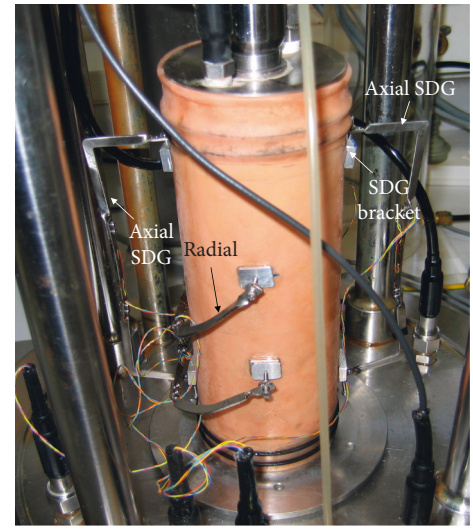

Figure 9: Triaxial specimen in the K_0 test.

actually consistent with the familiar correlation between K_0 and ϕ_{cv} [18]:

$$K_{0\,(NC)} = 1 - \sin \varnothing. \quad (5)$$

This correlation yields K_0 value of 0.40, which is only about 5% less than the measured one.

While the K_0 value determined using externally mounted LVDT appears satisfactory, the stress-strain behaviour (and hence stiffness) shows dramatic difference upon comparison with the response obtained from the internal SDG described in this paper. This can be seen clearly from Figure 12 and the closeup in Figure 13. The serious underestimation of the deformation modulus by the external LVDT is apparent; specifically, the values calculated for E are 29.3 MPa and 79.3 MPa for the external and SDG measurements, respectively. This result confirms that it is inevitable to use local deformation measurements for stiffness calculation.

6. Summary and Conclusions

This paper has presented a novel and versatile, local deformation device capable of resolving axial and radial strains down to 0.001% or better, a critical requirement for accurate determination of soil stiffness in triaxial tests. The device is called spring deformation gauge (SDG), which is based on securing a thin (e.g., 0.25 mm) metal strip from spring steel between two stiff, L-shaped legs made from stainless steel. The paper presented a closed form solution defining the influence of the geometry and Young's modulus of these two components on the performance of the SDG. The critical parameters of maximum measurable range and resolution can be readily controlled by varying the geometry of the SDG using the provided formula. The SDG is suitable for both axial and radial strain measurement.

In addition to the accuracy of the SDG and its ability to resolve small strain values, it has two main advantages over

Table 5: Resolution of the various devices used during the K_0 test.

Device	Axial SDG	Radial SDG	External LVDT	External volume change unit
Resolution	0.2 μm	0.075 μm	0.75 μm	1 mm^3
ε_a resolution (%)	1.0×10^{-3}		4.0×10^{-3}	
ε_r resolution (%)		1.0×10^{-3}		
ε_v resolution (%)				1.0×10^{-4}

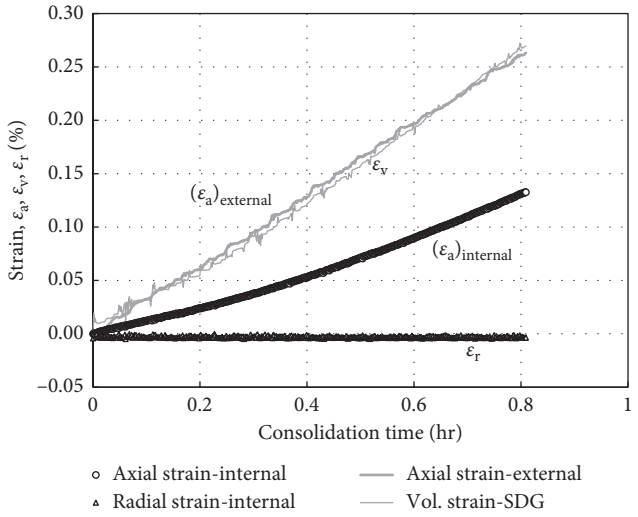

Figure 10: Response of the various transducers during K_0 consolidation.

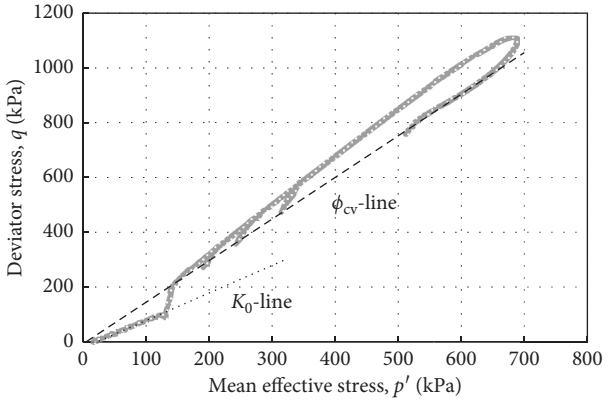

Figure 11: Relationship between K_0-line and f_{cv}-line.

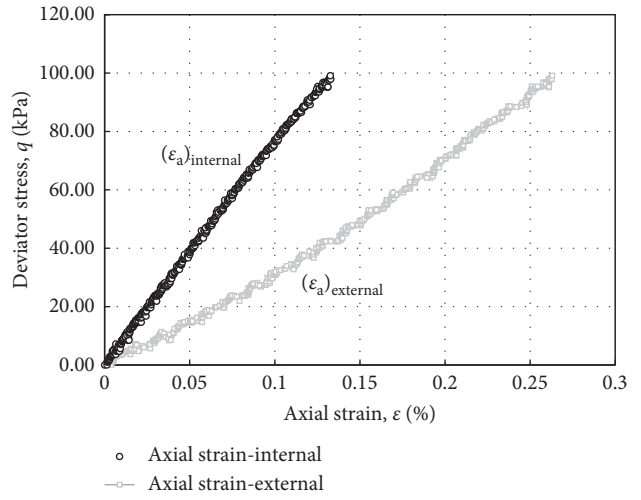

Figure 12: Stress-strain curve during K_0 consolidation.

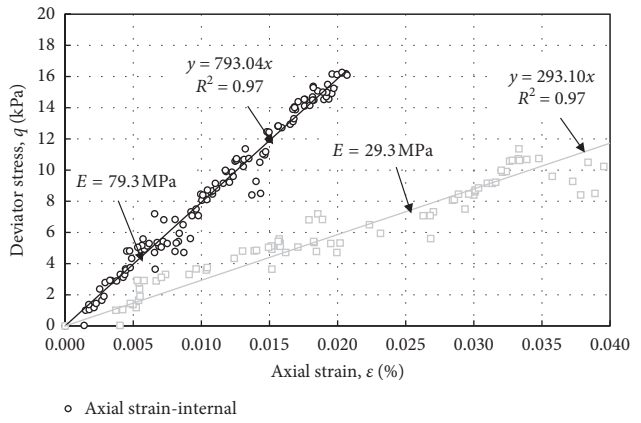

Figure 13: Influence of measuring technique on the deformation modulus.

many other transducers such as the LDT [8]: (1) the output of SDG is linear and (2) it can be connected to the specimen in a manner that it preserves the device once it goes out of range. The SDG can be used in water once the strain gauges glued to the spring steel strip are insulated by a proper nonconductive coating.

Performance of the SDGs was successfully investigated by performing a true K_0 test, followed by undrained shearing. The necessity of using internal strain measurement was manifested in this test through the deformation modulus, which was grossly underestimated using external LVDT compared with SDG.

Appendix

Proof of Equation (1)

In the following, the relationship between elongation of the spring strip of the deformation gauge and specimen axial deformation is deduced using the method of slope deflection. Two main assumptions are made in this regard: (1) deformations within the gauge are within the elastic range of all components and (2) curvature of the stiff legs of the gauge is negligible, compared with that of the spring. The following notations are used in the derivation below in association with Figure 2:

$(EI)_l$ = product of Young's Modulus and section inertia of the gauge leg

$(EI)_s$ = product of Young's Modulus and section inertia of the gauge spring

Let $\Delta L_{specimen}$ be the axial deformation of the triaxial specimen, which will lead to inward movement of points a and f of the gauge (δ_1 and δ_2 in Figure 2(a), respectively), such that

$$\delta_1 = \frac{\Delta L_{specimen}}{2}. \tag{A.1}$$

The two parameters that control the bending moment within the spring are δ_2 and θ. Applying the slope deflection equation at point c leads to

$$M_{cb} = \frac{6(EI)_l}{L_2}\left(\theta - \frac{\delta_2}{L_2}\right), \tag{A.2}$$

$$M_{cd} = \frac{2(EI)_s}{L_s}(2\theta - \theta), \tag{A.3}$$

$$M_{cb} + M_{cd} = 0. \tag{A.4}$$

Substituting equations (A.1) to (A.3) into equation (A.4) and rearranging lead to the following expression for the angle θ:

$$\theta = \frac{3(EI)_l}{6(EI)_l L_2 + 2(EI)_s (L_2/L_s) L_2}\Delta L_{specimen}. \tag{A.5}$$

The elongation of the spring can be calculated using Figure 2(b) as follows:

$$\Delta L_{spring} = \int_0^{2\theta}\left(R + \frac{t_s}{2}\right)d\theta - L_s, \tag{A.6}$$

$$\begin{aligned} \Delta L_{spring} &= 2R\theta + t_s\theta - L_s, \\ \Delta L_{spring} &= t_s\theta. \end{aligned} \tag{A.7}$$

Substituting equations (A.5) into (A.7) yields the following relationship between elongation of the spring and specimen axial deformation:

$$\Delta L_{spring} = \frac{3(EI)_l t_s}{6(EI)_l L_2 + 2(EI)_s (L_2/L_s) L_2}\Delta L_{specimen}. \tag{A.8}$$

Data Availability

The data used to support the findings of this study are included within the article.

Conflicts of Interest

The authors declare that they have no conflicts of interest.

Acknowledgments

The authors thank Prof. Boris Tarasov from the Centre for Offshore Foundation System at the University of Western Australia, who assisted with development of the gauge. The authors also thank Prince Sultan University for supporting the publication of this article.

References

[1] M. Goudarzy, D. König, and T. Schanz, "Small strain stiffness of granular materials containing fines," *Soils and Foundations*, vol. 56, no. 5, pp. 756–764, 2016.

[2] R. J. Jardine, M. J. Symes, and J. B. Burland, "The measurement of soil stiffness in the triaxial apparatus," *Géotechnique*, vol. 34, no. 3, pp. 323–340, 1984.

[3] D. C. F. Lo Presti, M. Jamiolkowski, A. Cavallaro, and O. Pallara, "Influence of reconsolidation techniques and strain rate on the stiffness of undisturbed clays from triaxial tests," *Geotechnical Testing Journal*, vol. 22, no. 3, pp. 211–225, 1999.

[4] D. C. F. Lo Presti, M. Jamiolkowski, A. Cavallaro, and O. Pallara, "Anisotropy of small strain stiffness in undisturbed and reconstituted clays," in *Proceedings of the 2nd International Symposium on Pre-failure Deformation Characteristics of Geomaterials*, pp. 3–10, Torino, Italy, September 1999.

[5] G. K. Scholey, J. D. Frost, D. C. F. Lo Presti, and M. Jamiolkowski, "A review of instrumentation for measuring small strains during triaxial testing of soil specimens," *Geotechnical Testing Journal*, vol. 18, no. 2, pp. 137–156, 1995.

[6] N. Zhalehjoo, A. Tolooiyan, R. Mackay, and D. Bodin, "The effect of instrumentation on the determination of the resilient modulus of unbound granular materials using advanced repeated load triaxial testing," *Transportation Geotechnics*, vol. 14, pp. 190–201, 2018.

[7] C. R. I. Clayton, S. A. Khatrush, A. V. D. Bica, and A. Siddique, "The use of hall effect semiconductors in geotechnical instrumentation," *Geotechnical Testing Journal*, vol. 12, no. 1, pp. 69–76, 1989.

[8] S. Goto, F. Tatsuoka, S. Shibuya, Y. Kim, and T. Sato, "A simple gauge for local small strain measurements in the laboratory," *Soils and Foundations*, vol. 31, no. 1, pp. 169–180, 1991.

[9] S. Yimsiri, K. Soga, and S. G. Chandker, "Cantilever-type local deformation transducer for local axial strain measurement in txriaxial test," *Geotechnical Testing Journal*, vol. 28, no. 5, article 11432, 2005.

[10] L. P. Mishu, *A study of stresses and strains in soil specimens in the triaxial test*, Ph.D. thesis, Purdue University, West Lafayette, IN, USA, 1966.

[11] C. C. Hird and P. C. Y. Yung, "The use of proximity transducers for local strain measurements in triaxial tests," *Geotechnical Testing Journal*, vol. 12, no. 4, pp. 292–296, 1989.

[12] S. Yimsiri and K. Soga, "A review of local strain measurement systems for triaxial testing of soils," *Journal of the Southeast Asian geotechnical society*, vol. 33, no. 1, pp. 41–52, 2002.

[13] Din 17221, *Hot Rolled Steels for Springs Suitable for Quenching and Tempering–Technical Delivery Conditions*, Springer, Berlin, Germany, 1988.

[14] MIT, March 2019, https://ocw.mit.edu/courses/materials-science-and-engineering/3-11-mechanics-of-materials-fall-1999/modules/MIT3_11F99_props.pdf.

[15] B. K. Menzies, H. Sutton, and R. E. Davies, "A new system for automatically simulating K_0 consolidation and K_0 swelling in the conventional triaxial cell," *Géotechnique*, vol. 27, no. 4, pp. 593–596, 1977.

[16] M. A. Ismail, H. A. Joer, and M. F. Randolph, "Cementation of porous materials using calcite precipitation," *Géotechnique*, vol. 52, no. 5, pp. 313–324, 2002.
[17] Meritt, Standard Pressure Volume Controller, 2015, https://perma.cc/H2Q8-Z75T.
[18] J. Jaky, "The coefficient of earth pressure at rest," *Journal for Society of Hungarian Architects and Engineers*, vol. 78, no. 22, pp. 355–358, 1944.